Gram-Scale One-Pot Synthesis of Highly Luminescent Blue Emitting Cd1− x Zn x S/ZnS Nanocrystals

ARTICLE *in* CHEMISTRY OF MATERIALS · AUGUST 2008

Impact Factor: 8.35 · DOI: 10.1021/cm801201x

4 AUTHORS, INCLUDING:

Wan Ki Bae
Korea Institute of Science and Technology
54 PUBLICATIONS **1,530** CITATIONS

Gram-Scale One-Pot Synthesis of Highly Luminescent Blue Emitting $Cd_{1-x}Zn_xS/ZnS$ Nanocrystals

Wan Ki Bae,[†] Min Ki Nam,[‡] Kookheon Char,*[,†] and Seonghoon Lee*[,‡]

School of Chemical and Biological Engineering, Center for Functional Polymer Thin Films, and School of Chemistry, NANO Systems Institute, National Core Research Center, Seoul National University, Seoul 151-747, Korea

Received May 1, 2008. Revised Manuscript Received June 17, 2008

We demonstrated a facile synthesis of highly luminescent blue emitting $Cd_{1-x}Zn_xS/ZnS$ core/shell structured nanocrystals (NCs) in straightforward and reproducible manner. The alloyed $Cd_{1-x}Zn_xS$ cores with homogeneity in both size and composition were prepared by introducing S precursors (S dissolved in the noncoordinating solvent (1-octadecene)) into the mixed solution of Cd−Oleate ($Cd(OA)_2$) and Zn−Oleate ($Zn(OA)_2$) at elevated temperature (300 °C). ZnS shells were successively overcoated on the prepared cores by the second injection of S precursors (S powder dissolved in tributylphosphine, TBPS) directly into the reactor with existing alloyed $Cd_{1-x}Zn_xS$ NC cores without any purification steps. The prepared NCs exhibit strong band edge emission with high photoluminescent quantum yield (PL QY, up to 80%) and narrow spectral bandwidth (fwhm < 25 nm), which is believed to originate from the successful growth of ZnS shell layers on the $Cd_{1-x}Zn_xS$ cores and the interfacial compatibility between $Cd_{1-x}Zn_xS$ cores and the ZnS shell layers through the intradiffusion of Zn atoms from the ZnS shells into the $Cd_{1-x}Zn_xS$ cores during the shell formation reaction. The emission wavelength (PL $\lambda_{max.}$) of $Cd_{1-x}Zn_xS/ZnS$ core/shell NCs was finely tuned from violet (415 nm) to blue (461 nm) by adjusting the amount of S precursors in the first injection (S in 1-octadecene) and thus changing actual Cd content ratio in the alloyed $Cd_{1-x}Zn_xS$ cores ($0.49 \leq x \leq 0.76$). Furthermore, multigram (3 g) scale production of $Cd_{1-x}Zn_xS/ZnS$ core/shell NCs with narrow size distribution and spectral bandwidth was also demonstrated.

Introduction

Semiconductor nanocrystals (NCs) have been enthusiastically exploited not only because of their unique properties depending on their size which is referred as the "quantum confinement effect (QCE)"[1−3] but also because of their potential applications such as light emitting diodes,[4−7] photovoltaic devices,[8−10] lasers,[11−13] and biological markers.[14−16] Particularly, the synthesis and design of highly luminescent NCs have been one of the most important issues for the fundamental understanding of nanosized materials as well as the successful realization of practical applications. Ever since CdSe NCs with uniform size and shape have been demonstrated,[17] significant progress in the synthesis of NCs with superb optical properties has been achieved through the passivation of the surfaces of NCs with organic or inorganic overlayers.[18−25] Moreover, the synthetic procedures have been also optimized and simplified, and NCs with complex structure can now be easily prepared through the one-pot

* Corresponding authors. E-mail: shnlee@snu.ac.kr (S.L.), khchar@plaza.snu.ac.kr (K.C.).
[†] School of Chemical and Biological Engineering.
[‡] School of Chemistry.

(1) Brus, L. *J. Phys. Chem.* **1986**, *90*, 2555–2560.
(2) Murray, C. B.; Kagan, C. R.; Bawendi, M. G. *Annu. Rev. Mater. Sci.* **2000**, *30*, 545–610.
(3) Alivisatos, A. P. *Science* **1996**, *271*, 933–9377.
(4) Colvin, V. L.; Schlamp, M. C.; Alivisatos, A. P. *Nature* **1994**, *370*, 354–357.
(5) Coe, S.; Woo, W. K.; Bawendi, M.; Bulovic, V. *Nature* **2002**, *420*, 800–803.
(6) Achermann, M.; Petruska, M. A.; Kos, S.; Smith, D. M.; Koleske, D. D.; Klimov, V. I. *Nature* **2004**, *429*, 642–646.
(7) Lee, J.; Sundar, V. C.; Heine, J. R.; Bawendi, M. G. *Adv. Mater.* **2000**, *12*, 1102–1105.
(8) Huynh, W. U.; Dittmer, J. J.; Alivisatos, A. P. *Science* **2002**, *295*, 2425–2427.
(9) Gur, I.; Fromer, N. A.; Geier, M. L.; Alivisatos, A. P. *Science* **2005**, *310*, 462–465.
(10) Plass, R.; Pelet, S.; Krueger, J.; Gratzel, M.; Bach, U *J. Phys. Chem. B* **2002**, *106*, 7578–7580.
(11) Klimov, V. I.; Mikhailovsky, A. A.; Xu, S.; Malko, A.; Hollingsworth, J. A.; Leatherdale, C. A.; Eisler, H. J.; Bawendi, M. G. *Science* **2000**, *290*, 314–317.
(12) Kazes, M.; Lewis, D. Y.; Ebenstein, Y.; Mokari, T.; Banin, U. *Adv. Mater.* **2002**, *14*, 317.
(13) Malko, A. V.; Mikhailovsky, A. A.; Petruska, M. A.; Hollingsworth, J. A.; Htoon, H.; Bawendi, M. G.; Klimov, V. I. *Appl. Phys. Lett.* **2002**, *81*, 1303–1305.
(14) Bruchez, M.; Moronne, M.; Gin, P.; Weiss, S.; Alivisatos, A. P. *Science* **1998**, *281*, 2013–2016.
(15) Chan, W. C. W.; Nie, S. M. *Science* **1998**, *281*, 2016–2018.
(16) Medintz, I. L.; Uyeda, H. T.; Goldman, E. R.; Mattoussi, H. *Nat. Mater.* **2005**, *4*, 435–446.
(17) Murray, C. B.; Norris, D. J.; Bawendi, M. G. *J. Am. Chem. Soc.* **1993**, *115*, 8706–8715.
(18) Qu, L.; Peng, X. *J. Am. Chem. Soc.* **2002**, *124*, 2049–2055.
(19) Wuister, S. F.; Houselt, A.; Donega, C. M.; Vanmaekelbergh, D.; Meijerink, A. *Angew. Chem., Int. Ed.* **2004**, *43*, 3029–3033.
(20) Dabbousi, B. O.; Rodriguez-Viejo, J.; Mikulec, F. V.; Heine, J. R.; Mattoussi, H.; Ober, R.; Jensen, K. F.; Bawendi, M. G. *J. Phys. Chem. B* **1997**, *101*, 9463–9475.
(21) Li, J. J.; Wang, Y. A.; Guo, W.; Keay, J. C.; Mishima, T. D.; Johnson, M. B.; Peng, X. *J. Am. Chem. Soc.* **2003**, *125*, 12567–12575.
(22) Reiss, P.; Bleuse, J.; Pron, A. *Nano Lett.* **2002**, *2*, 781–784.
(23) Talapin, D. V.; Mekis, I.; Gotzinger, S.; Kornowski, A.; Benson, O.; Weller, H. *J. Phys. Chem. B* **2004**, *108*, 18826–18831.
(24) Talapin, D. V.; Rogach, A. L.; Kornowski, A.; Haase, M.; Weller, H. *Nano Lett.* **2001**, *1*, 207–211.
(25) Xie, R.; Kolb, U.; Li, J.; Basche, T.; Mews, A *J. Am. Chem. Soc.* **2005**, *127*, 7480–7488.

10.1021/cm801201x CCC: $40.75
Published on Web 08/02/2008

synthetic method.[21,25−28] Thanks to those innovations in designing nanomaterials and their synthesis, applications to light-emitting diodes, lasers, and biological labeling would be possible for practical commercialization.

However, the achievements reported in the synthesis of NCs have been relatively limited on semiconductor NCs with photoluminescent emission from 510 nm (green) to 640 nm (red), which do not cover the violet to blue emission region. Recently, several methods for the synthesis of blue emitting NCs have been demonstrated with CdSe,[29,30] CdS,[31,32] $CdSe_{1-x}S_x$,[33] $Cd_{1-x}Zn_xSe$,[34] and $Cd_{1-x}Zn_xS$[35] through the moderate control of reaction conditions such as type of surfactants or reaction temperature, but the suggested synthetic schemes do not guarantee blue emitting NCs with high photoluminescent quantum efficiency (PL QY) and narrow spectral distribution in the wide range of the blue emission region (410−460 nm), which are the critical elements for applications to light emitting diodes or lasers.[36−42] Furthermore, the synthesis of core/shell structured blue emitting NCs is typically rather difficult because it requires the elaborate control of the formation of smaller cores and it also involves synthetic procedures of multiple steps to suppress further reaction of remaining precursors (mainly Cd or Se) during the shell formation, which would otherwise cause the drastic red-shift in emission wavelength (typically 20 to 40 nm of red-shift). Synthetic methods producing reasonable amount of blue emitting NCs with high photoluminescent quantum efficiency (PL QY) are quite limited so far.

Here, we report one-pot synthesis of highly luminescent blue emitting $Cd_{1-x}Zn_xS$/ZnS core/shell structured NCs through the second injection of S precursors directly into the reactor with existing alloyed $Cd_{1-x}Zn_xS$ quantum dot cores without any purification steps. The prepared NCs show high PL QY (up to 80%) with narrow spectral bandwidth (fwhm < 25 nm). The emission wavelength ranging from 410 to 460 nm can be finely tuned by adjusting the amount of S precursors in the first injection (S in 1-octadecene) and thus changing actual Cd content ratio between Cd and Zn in the alloyed $Cd_{1-x}Zn_xS$ cores ($0.49 \leq x \leq 0.76$). We also demonstrate the scale-up capabilty of the synthesis of blue-emitting NCs in grams order range (e.g., 3 g production per one-pot synthesis is demonstrated).

Experimental Section

Chemicals. Cadmium oxide (CdO, 99.99%), zinc acetate ($Zn(acet)_2$, 99.9%, powder), sulfur (99.9%, powder), tributylphosphine (TBP, 97%), oleic acid (OA, 99%), and 1-octadecene (1-ODE, 90%) were used as purchased from Aldrich. 9,10-Diphenylanthracene (99%) was purchased from Fluka.

Synthesis of $Cd_{1-x}Zn_xS$/ZnS Core/Shell Structured Nanocrystals (1.2 g scale). The synthetic procedures and characterization techniques are similar with those reported previously.[28] As a typical synthetic procedure, 1 mmol of CdO, 10 mmol of $Zn(acet)_2$, and 7 mL of OA were placed in a 100 mL round flask. The mixture was heated to 150 °C, degassed under 100 mtorr pressure for 20 min, filled with N_2 gas, added with 15 mL of 1-ODE, and further heated to 300 °C to form a clear mixture solution of $Cd(OA)_2$ and $Zn(OA)_2$. At this temperature, 2 mmol of S powder dissolved in 3 mL of 1-ODE was quickly injected into the reaction flask. After the first injection of S precursors, the temperature of the reaction flask was elevated to 310 °C for further growth of $Cd_{1-x}Zn_xS$ cores. After the elapse of 8 min of reaction, 8 mmol of S powder dissolved in TBP (TBPS) were introduced into the reactor to overcoat existing $Cd_{1-x}Zn_xS$ cores with ZnS shells without any purification steps. Aliquots of NCs were taken during the reaction to analyze the development of NCs. After the reaction was completed, the temperature was cooled down to room temperature. NCs were extracted and purified by adding 20 mL of chloroform and an excess amount of acetone (done twice); then they were redispersed in chloroform or hexane for further characterization. To adjust the optical properties of NCs, we varied the amount of S precursors in the first injection (1.2, 1.5, 1.7, 2.0, 2.2, and 2.7 mmol in 3 mL of 1-ODE), maintaining all the other parameters such as the amounts of CdO, $Zn(acet)_2$, OA, S (with the amount used in the second injection fixed), 1-ODE, or TBP, reaction temperature, and reaction time, constant. Using this successful same synthetic method applied to the production of 1.2 g of blue emitting NCs, we were able to produce 3 g of NCs (~3 times NCs as much) by simply scaling up all the amounts of chemicals used in the reaction three times.

Characterization. Room temperature UV−vis absorption spectra were measured with an Agilent 8454 UV−vis diode array spectrometer. Photoluminescence (PL) spectra were collected on an ACTON spectrometer. The photoluminescent quantum yields (PL QY) of the NCs were measured and estimated by comparing their fluorescence intensities with those of primary standard dye solutions (9,10-diphenylanthracene, QY = 91% in ethanol) at the same optical density (O.D. = 0.05) at the same excitation wavelength (370 nm). The TEM images of the NCs were obtained using a JEOL JSM-890 at 200 KV to analyze their average size and size distribution. The energy dispersive X-ray (EDX) spectra of NCs were acquired through Si−Li detector of Oxford INCA Energy attached on the main body of the TEM. Low-coverage samples were prepared by placing a drop of a dilute hexane dispersion of NCs on a copper grid (300 mesh) coated with an amorphous carbon film.

Thermal Annealing Experiment. The thermal annealing experiments were performed by elevating the temperature of the reactors containing $Cd_{1-x}Zn_xS$/ZnS NCs (grown at 250 °C for 30 min) to 310 °C without any purification and maintaining at that temperature. The temperature of reactors was increased from 250 °C to 310 °C

(26) Kim, J. I.; Lee, J. *Adv. Funct. Mater.* **2006**, *16*, 2077–2082.
(27) Lim, J.; Jun, S.; Jang, E.; Baik, H.; Kim, H.; Cho, J. *Adv. Mater.* **2007**, *19*, 1927–1932.
(28) Bae, W. K.; Char, K.; Hur, H.; Lee, S. *Chem. Mater.* **2008**, *20*, 531–539.
(29) Jun, S.; Jang, E. *Chem. Commun.* **2005**, *36*, 4616–4618.
(30) Kudera, S.; Zanella, M.; Giannini, C.; Rizzo, A.; Li, Y.; Gigli, G.; Cingolani, R.; Ciccarella, G.; Spahl, W.; Parak, W. J.; Manna, L. *Adv. Mater.* **2007**, *19*, 548–552.
(31) Yu, W. W.; Peng, X. *Angew. Chem., Int. Ed.* **2002**, *41*, 2368–2371.
(32) Steckel, J. S.; Zimmer, J. P.; Coe-Sullivan, S.; Stott, N. E.; Bulovic, V.; Bawendi, M. G. *Angew. Chem., Int. Ed.* **2004**, *43*, 2154–2158.
(33) Jang, E.; Jun, S.; Pu, L. *Chem. Commun.* **2003**, *24*, 2964–2965.
(34) Zhong, X.; Zhang, Z.; Liu, S.; Han, M.; Knoll, W. *J. Phys. Chem. B* **2004**, *108*, 15552–15559.
(35) Zhong, X.; Feng, Y.; Knoll, W.; Han, M. *J. Am. Chem. Soc.* **2003**, *125*, 13559–13563.
(36) Rizzo, A.; Li, Y.; Kudera, S.; Sala, F. D.; Zanella, M.; Parak, W. J.; Cingolani, R.; Manna, L.; Gigli, G. *Appl. Phys. Lett.* **2007**, *90*, 051106.
(37) Tan, Z.; Zhang, F.; Zhu, T.; Xu, J.; Wang, A. Y.; Dixon, J. D.; Li, L.; Zhang, Q.; Mohney, E.; Ruzyllo, J. *Nano Lett.* **2007**, *7*, 3803–3807.
(38) Li, Y.; Rizzo, A.; Cingolani, R.; Gigli, G. *Adv. Mater.* **2006**, *18*, 2545–2548.
(39) Anikeeva, P. O.; Halpert, J. E.; Bawendi, M. G.; Bulovic, V. *Nano Lett.* **2007**, *7*, 2196–2200.
(40) Ali, M.; Chattopadhyay, S.; Nag, A.; Kumar, A.; Sapra, S.; Chakraborty, S.; Samara, D. D. *Nanotechnology* **2007**, *18*, 075401.
(41) Sun, Q.; Wang, A.; Li, L. S.; Wang, D.; Zhu, T.; Xu, J.; Yang, C.; Li, Y. *Nat. Phonics* **2007**, *1*, 717–722.
(42) Chan, Y.; Steckel, J. S.; Snee, P. T.; Caruge, J. M.; Hodgkiss, J. M.; Nocera, D. G.; Bawendi, M. G. *Appl. Phys. Lett.* **2005**, *86*, 073102.

Table 1. Size, Composition, PL Emission Wavelength ($\lambda_{max.}$), and PL QY of $Cd_{1-x}Zn_xS$ Core NCs Prepared by Different Amounts of the First S Injection[a] and $Cd_{1-x}Zn_xS/ZnS$ Core/Shell NCs Prepared by the Second Injection of S Precursors[b,c]

	$Cd_{1-x}Zn_xS$ (core)					$Cd_{1-x}Zn_xS/ZnS$ (core/shell)			
first S injection	Cd:Zn	size	PL $\lambda_{max.}$	QY (Φ)	second S injection	Cd:Zn	size	PL $\lambda_{max.}$	QY (Φ)
1.2mmol	0.76:0.24	5.4 nm	467nm	<5%	8mmol	0.14:0.86	9.0 nm	461nm	42%
1.5mmol	0.72:0.28	5.1 nm	460nm	<5%	8mmol	0.15:0.85	8.5 nm	450nm	62%
1.7mmol	0.70:0.30	5.2 nm	450nm	<5%	8mmol	0.16:0.84	8.7 nm	443nm	70%
2.0mmol	0.58:0.42	4.7 nm	441nm	<5%	8mmol	0.16:0.84	8.2 nm	433nm	81%
2.2mmol	0.51:0.49	4.5 nm	429nm	<5%	8mmol	0.16:0.84	8.5 nm	422nm	68%
2.7mmol	0.49:0.51	4.3 nm	423nm	<5%	8mmol	0.15:0.85	7.5 nm	415nm	48%

[a] 1.2, 1.5, 1.7, 2.0, 2.2, and 2.7 mmol. [b] 8 mmol of S in 3 mL of TBP. [c] Reaction conditions: Cd 1 mmol, Zn 10 mmol, OA 7 mL, 1-ODE 15 mL, $T_{Injection}$ 300 °C, and T_{Growth} 310 °C.

with a rate of 60 °C/min. The sampling aliquots were taken during the thermal annealing experiments and were purified twice and then were dispersed in chloroform for further analysis.

Photostability Test. The photostability test of prepared NCs was conducted by analyzing the PL intensity of NC dispersions obtained at different UV exposure intervals. NC dispersions (dispersed in chloroform) were exposed under continuous UV (354 nm) irradiation with the strength of 1.5 W/cm^2 under the laboratory condition.

Time-resolved PL Decay. The NCs dispersed in toluene were used for time-resolved PL decay experiments. The output from a home-built cavity-dumped mode-locked Ti:sapphire laser (740 nm, 500 kHz, 20 fs) was doubled to 370 nm through a 100-μm thick BBO crystal for the excitation of the NCs. A lens (f = 150 mm) and a parabolic mirror (f = 101.6 mm) were used to focus excitation light and to collect PL in the backscattering geometry, respectively. The PL spectra were taken with a TE-cooled CCD (Andor, DU-401) mounted on a 30 cm monochromator (Acton, SP-300, 150 grooves/mm) with a spatial 2 nm resolution. The time-resolved PL was measured with time-correlated single photon counting (TCSPC) system equipped with the microchannel plate photomultiplier tube (Hamamatsu, R3809-51). The instrument response function was 50 ps (fwhm), providing 10 ps time resolution with deconvolution.[43]

Results and Discussion

$Cd_{1-x}Zn_xS/ZnS$ core/shell structured NCs were prepared through the second injection of S precursors directly into a hot mixed solution of Cd−Oleate ($Cd(OA)_2$) and Zn−Oleate ($Zn(OA)_2$). After the first injection of S precursors (S powder in noncoordinating solvent 1-ODE), $Cd_{1-x}Zn_xS$ NCs nucleate and grow in the given reaction conditions. When the highly reactive S precursor such as S powder dissolved in 1-ODE was used, alloyed $Cd_{1-x}Zn_xS$ cores were formed rather than the cores with composition gradient which were typically produced by S precursors with lower reactivity such as S-bound ligands (TOPS or TBPS) or S-containing chemicals (alkylthiols). The alloyed $Cd_{1-x}Zn_xS$ cores prepared by highly reactive S precursor (S powder dissolved in 1-ODE) takes spherical shapes together with narrow size distribution and almost the same compositions, which are confirmed by TEM and narrow PL emission spectra (fwhm < 20 nm). Since Cd^{2+} has weaker binding energy with oleic acid compared with Zn^{2+},[44] $Cd(OA)_2$ reacts with S faster than $Zn(OA)_2$, and thus the $Cd_{1-x}Zn_xS$ alloyed cores have relatively higher Cd contents ($0.49 \le x \le 0.76$), even considering the initial Cd to Zn feed ratio is 1 to10 (see Table 1). Most of the first injected S precursor was consumed in 8 min of reaction, and then the second S precursors, S powder dissolved in TBP (TBPS), were sequentially introduced directly into the reactor without any purification to form ZnS overlayers on the surface of alloyed $Cd_{1-x}Zn_xS$ cores. The prepared $Cd_{1-x}Zn_xS/ZnS$ core/shell structured NCs have narrow size distribution and maintain spherical shapes, but their general morphological shape is not as spherical as the cores only.

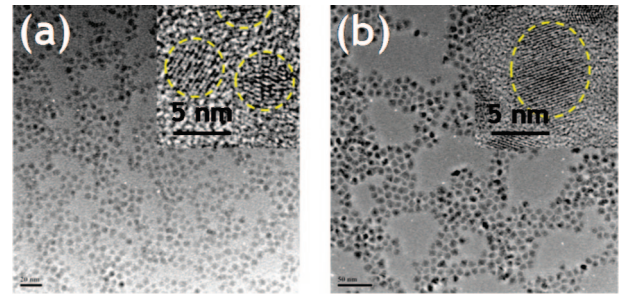

Figure 1. HRTEM images of (a) alloyed $Cd_{0.7}Zn_{0.3}S$ cores obtained after 8 min of reaction from the first S injection and (b) $Cd_{0.7}Zn_{0.3}S/ZnS$ core/shell structured nanocrystals obtained after 30 min of reaction from the second S injection.

Figure 1a,b shows the HRTEM images of $Cd_{0.7}Zn_{0.3}S$ cores only and $Cd_{0.7}Zn_{0.3}S/ZnS$ core/shell NCs, respectively. Both of NCs have high crystallinity (Wurzite structure) and narrow size distribution. Regardless of the Cd content in the core ($0.49 < x < 0.76$), the alloyed core NCs or core/shell NCs show similar shape and crystallinity and narrow size distribution. We noticed that the alloyed core NC diameter was about 5.2 nm (±0.5 nm) and that the core/shell NC diameter was increased to about 8.7 nm (±0.5 nm) after the shell formation process was done in a given reaction condition. The increased shell thickness corresponds to the formation of three layers of ZnS on the top of the core surface, which is also consistent with the EDX analysis based on the composition ratio of Cd to Zn.

Figure 2 shows the optical spectra of a $Cd_{1-x}Zn_xS$ core and $Cd_{1-x}Zn_xS/ZnS$ core/shell NCs taken at different reaction times. The PL spectrum (denoted in a dotted line) of the $Cd_{1-x}Zn_xS$ core shows the broad emission in a visible region (450 to 700 nm) originating from the surface states and the weak narrow Gaussian-shaped band edge emission around 440 nm. With the shell formation process by the addition of the second S precursor, TBPS, however, the surface-state emissions were strongly suppressed and only the band edge PL emissions were drastically enhanced. These PL spectra were also shown in a solid line in Figure 2. The photoluminescence quantum yield (PL QY (Φ)) of core−shell

(43) Jung, S. W.; Park, W. I.; Cheong, H. D.; Yi, G.; Jang, H. M.; Hong, S.; Joo, T. *Appl. Phys. Lett.* **2002**, *80*, 1924.
(44) Phillips, J. C.; Van Vechten, J. A. *Phys. Rev. Lett.* **1969**, *22*, 705–708.

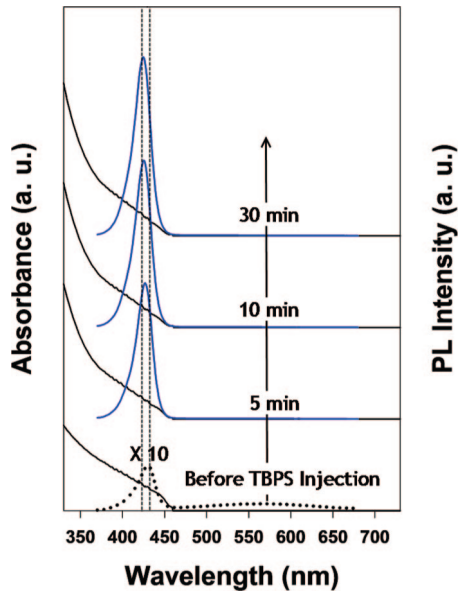

Figure 2. UV−vis and PL spectral evolution of nanocrystals acquired during the reaction (8 min of core formation reaction (denoted in a dotted line) from the first S injection and 5, 10, and 30 min of shell formation reaction (denoted in a solid line) from the second S injection (from the bottom), respectively).

structured NCs synthesized by the second injection of S precursor was measured to be up to 80%, which is the highest value among those of blue emitting quantum dots reported so far. We believe that this remarkable enhancement in optical properties is due to the successful surface passivation of the cores with ZnS shells of wider band gap. The ZnS shells structurally passivate the dangling bonds on the surface of cores and also energetically suppress the leakage of excitons from the cores into the shell because of its wider band gap than that of the core and so the $Cd_{1-x}Zn_xS$/ZnS NCs emit the strong band edge photoluminescence originating from the $Cd_{1-x}Zn_xS$ cores. Interestingly, the PL emission spectra of the $Cd_{1-x}Zn_xS$/ZnS core/shell NCs in this study were blue-shifted by 8 nm ± 2 nm when compared with the emission from the core itself, which was opposite tendency to the core/shell QDs produced by the epitaxial ZnS shell growth on CdSe or CdS cores previously reported (red-shift was observed by others).[32]

To understand these intriguing observations (i.e., significant increase in PL QY and the blue-shift of PL $\lambda_{max.}$) during the ZnS shell formation, we performed the ZnS shell overcoating at different reaction temperature (from 250 °C to 310 °C) with the other reaction conditions remaining the same (Figure 3). In the case of thermal annealing of alloyed $Cd_{1-x}Zn_xS$ cores without the second injection of S precursors (TBPS), the $Cd_{1-x}Zn_xS$ core NCs do not show any improvement in PL QY. No noticeable change in PL emission intensity is also observed. This is quite different from the previous report: blue-shift in PL wavelength and the improvement of PL QY triggered by further alloying progress caused by thermal annealing in $Cd_{1-x}Zn_xS$ NCs.[35] The NCs that experienced the shell formation by the second injection of S precursors, however, show the blue-shift in PL emission and highly enhanced PL QY which depend on the reaction temperature. The PL emission of NCs obtained at the reaction temperature above 280 °C is blue-shifted about 8 nm (from 450 to 442 nm) within the elapse of 2 h while that of NCs obtained at a reaction proceeded at 250 °C is blue-shifted only 2 nm. However, taking that the NCs obtained after the elapse of 30 min of ZnS-overcoating reaction have similar size (8.3 ± 0.3 nm) and uniform spherical shape regardless of reaction temperature into account, it is considered that the blue-shift in PL emission originates from the intradiffusion of Zn atoms from the ZnS shell layer into the $Cd_{1-x}Zn_xS$ cores, which has also been observed in the case of CdSe/ZnSe at high reaction temperature above 300 °C.[34] The intradiffusion of Zn atoms from the ZnS shell layer into the $Cd_{1-x}Zn_xS$ cores can be explained as follows. As Zn atoms in the shell layer migrate into the core region, the relative content of Cd in the core region decreases and thus the band gap of the cores increases (~50 meV corresponding to ~8 nm shift) depending on the change in composition in the core region (i.e., Cd to Zn). The blue-shift in PL emission (~8 nm shift) corresponds to the increase in Zn component (x) (~0.04 increase) in bulk $Cd_{1-x}Zn_xS$ or alloyed $Cd_{1-x}Zn_xS$ nanocrystals.[35] This increase in Zn is achieved through the

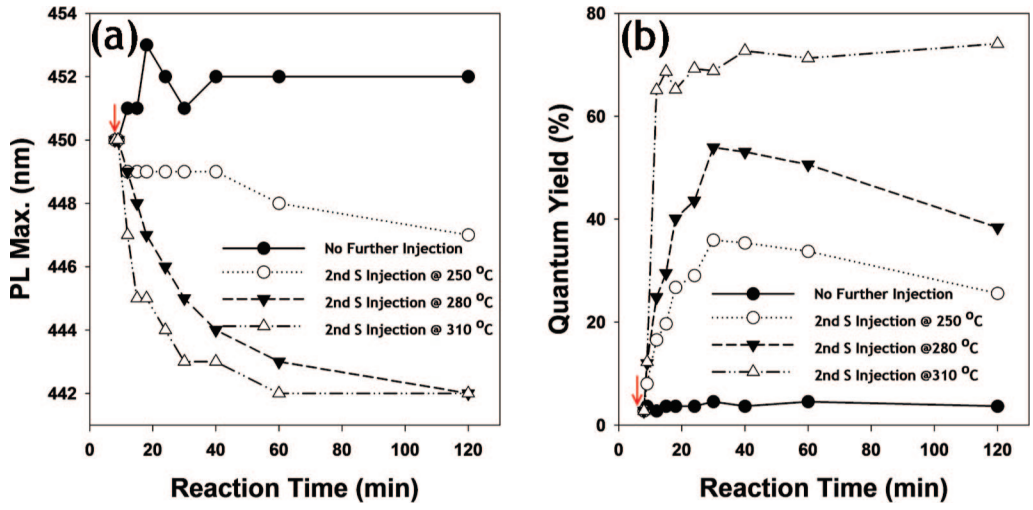

Figure 3. (a) PL emission wavelengths ($\lambda_{max.}$) during the shell formation as a function of reaction time at different reaction temperatures (red arrows denote the time of the second injection of S precursors) and (b) PL QY vs reaction time at different reaction temperatures. The meanings of the various marks are described inside the figure.

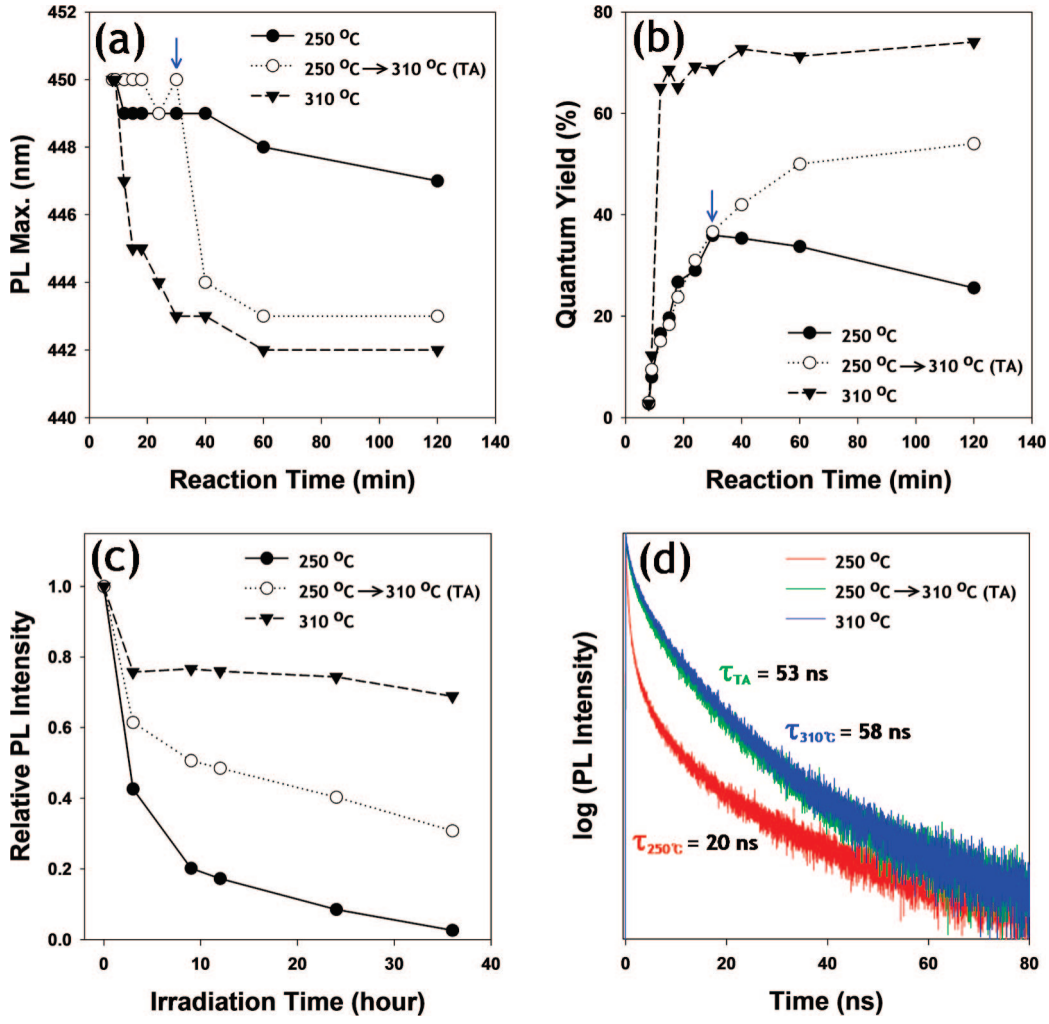

Figure 4. (a) PL emission wavelengths (λ_{max}) of NCs during the thermal treatment experiment, (blue arrows denote the increase of reaction temperature for the thermal treatment experiments) and (b) PL QY vs reaction time at different reaction temperature. (c) Relative PL intensity for each sample during the photostability test, and (d) time-resolved PL decay of different NCs. Notation in the figure carries the usual meaning as written.

intradiffusion. We believe that the increase in Zn content in the core region leads the PL emission to shift to shorter wavelength. As the reaction temperature is increased above 250 °C, the diffusion of Zn atoms from the shell layer into the core region is highly enhanced.

NCs with ZnS shell layers formed by the second injection of S precursors exhibit significant enhancement in PL QY. As the reaction temperature is increased, the core/shell structured NCs show the faster rise in PL QY as a function of reaction time (normally after 30−40 min reaction time, $\Phi = 71\%$, 53%, and 35% at 310 °C, 280 °C, and 250 °C of reaction temperature, respectively). The core/shell NCs prepared at 310 °C show strong PL emission at room temperature with intensity 3 times larger than that of CdS/ZnS quantum dots with the same ZnS shell thickness.[32] We consider that the high PL QY of $Cd_{1-x}Zn_xS/ZnS$ NCs is due to the structural properties of the interface between the core and the shell. The alloyed $Cd_{1-x}Zn_xS$ cores have less lattice mismatch with the ZnS overlayers compared with CdS cores with an abrupt ZnS shell, and thus they have less mechanical stress between the core and the shell, leading to facile epitaxial growth of ZnS layers on the top of the alloyed core surface rather than forming ZnS clusters on the core surfaces.[20] Moreover, the interface between the core and the shell seems to become more diffuse by the thermal annealing (i.e., the migration of Zn atoms form the shell to the core region) during the shell formation reaction at higher reaction temperature (310 °C).

To better understand the effect of the migration of Zn atoms from the shell into the core on the optical properties of NCs (i.e., PL QY and photostability), we annealed them thermally at 310 °C just after the shell formation step was done at 250 °C.

During the thermal annealing at 310 °C, the core/shell NCs show the blue-shift (∼ 8 nm) in the PL emission although no visible change in both size and shape of those NCs was observed, indicating the migration of Zn atoms from the ZnS shell into the $Cd_{1-x}Zn_xS$ core as shown in Figure 4a. This indicates that intradiffusion of the Zn atoms toward the core is thermally activated. In case of the core/shell NCs prepared at 250 °C with the second injection of S precursors and no further temperature increase, the PL QY of those increased up to 35% for the initial 30 min of reaction, and then it starts to decrease down to 25% after 30 min and then stays constant as shown in Figure 4b. In contrast, the core/shell NCs prepared at 250 °C through 30 min of reaction and followed by the thermal annealing at 310 °C show the continuous increase in PL QY throughout the entire thermal annealing

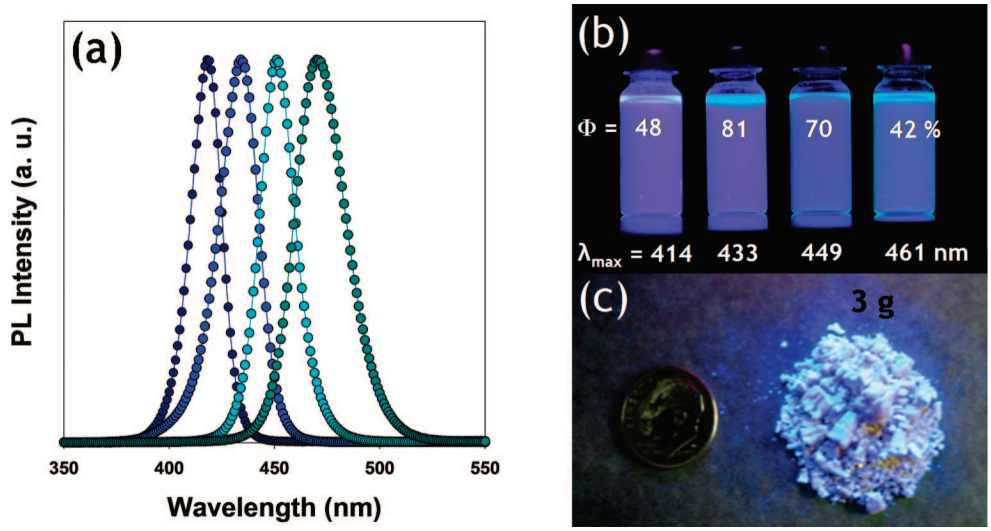

Figure 5. (a) PL emission spectra of $Cd_{1-x}Zn_xS/ZnS$ core/shell NCs, (b) a photograph of NC dispersions ($\lambda_{max.}$ = 414, 433, 449, and 461 nm from the left), and (c) a photograph of NC powder obtained by 3 g-scale synthesis.

process, but the ultimate PL QY of those can not reach as high as that of core/shell NCs prepared initially at 310 °C as shown, the ones denoted with ○ symbols in Figure 4b. Moreover, the NCs prepared above 250 °C are much more photostable under continuous UV irradiation (at 354 nm with a dosage of 1.5 W/cm^2), compared with the NCs prepared at 250 °C, as shown in Figure 4c. The difference in emission characteristics between the thermally annealed NCs at 310 °C and the NCs prepared at 250 °C without further thermal annealing at 310 °C is also observed in the time-resolved PL decay profiles as shown in Figure 4d. The thermally annealed NCs at higher temperature (above 250 °C) show longer PL lifetimes (τ_{TA} = 53 ns, TA, thermal annealing, and $\tau_{310°C}$ = 58 ns), compared with that of NCs prepared at 250 °C ($\tau_{250°C}$ = 20 ns), which is considered to be due to the suppression of the fast nonradiative exciton decay pathway (<ns). From these comparisons mentioned above, we can attribute the homogeneous intradiffusion of Zn atoms from the shell layer into the core by the thermal annealing to one of main reasons for improved PL QY and better photostability. And the migration of Zn atoms inward makes the interface between $Cd_{1-x}Zn_xS$ core and ZnS shell diffuse, relaxing the structural stress at the interface and eventually leading to high PL QY together with improved photostability. The difference in PL QY and photostability between the NCs prepared at 250 °C with further thermal treatment at 310 °C and the NCs prepared solely at 310 °C are thought to be due to the uniformity in shell thickness and/or the homogeneity in shell composition.

Figure 5a shows various PL emission spectra of $Cd_{1-x}Zn_xS/ZnS$ core/shell NCs prepared at 310 °C in these experiments. The emission spectra are finely tuned by simply changing the amount of S precursors introduced at the first injection (Table 1). As the amount of S precursors (S dissolved in 1-ODE, more reactive precursor) in the first injection is reduced, the $Cd_{1-x}Zn_xS$ cores with relatively higher Cd content were obtained. This is because the introduction of larger amounts of S precursors triggers spawning more nuclei rather than forming larger cores.[28] Since the amount of Cd and Zn used for the reaction were fixed (1 and 10 mmol for Cd and Zn precursors, respectively), the increase in nucleation number results in the decrease in Cd content in each $Cd_{1-x}Zn_xS$ core. Since the $Cd_{1-x}Zn_xS$ cores prepared in this condition have larger radii (4.3−5.4 nm) than the bulk Bohr exciton radius of ZnS (2.2 nm) or CdS (3.0 nm), they are in the weak quantum confinement regime (QCE) and their optical properties are less affected by the size or size distribution but strongly affected by the compositions.[35] Consequently, we could obtain the $Cd_{1-x}Zn_xS/ZnS$ core/shell structured NCs with various emission wavelengths ($\lambda_{max.}$) ranging from violet (415 nm) to blue (461 nm) by the adjustment of composition in the core. All the NCs obtained after the shell formation show the strong band edge emission with a narrow spectral bandwidth (fwhm < 25 nm).

In a typical synthesis, 1.2 g of NCs was obtained at the final step through purification by EtOH (or acetone) and $CHCl_3$ solvents twice. The amount of highly luminescent blue emitting $Cd_{1-x}Zn_xS/ZnS$ core/shell structured nanocrystal final products can be easily scaled up to several grams as shown in Figure 5c by simply multiplying the amount of reactants. The blue emitting $Cd_{1-x}Zn_xS/ZnS$ core/shell structured NCs obtained in 3 g-synthetic scale also maintain high PL QY (its QY varies within ±10% compared with the PL QY of NCs obtained in 1.2 g-synthetic scale) with almost the same PL emission wavelength (within ± 5 nm) and narrow spectral bandwidth (fwhm < 25 nm).

Figure 6 schematically depicts the synthetic procedures and the proposed structures of alloyed $Cd_{1-x}Zn_xS$ core NCs and $Cd_{1-x}Zn_xS/ZnS$ core/shell NCs on the basis of results obtained so far. After the first injection of S precursors (S dissolved in 1-ODE), $Cd_{1-x}Zn_xS$ alloyed cores nucleate and grow rapidly. The prepared cores are found to be uniform in size and composition, which is confirmed by TEM and spectral distribution analysis with EDX. From thermal annealing performed on $Cd_{1-x}Zn_xS$ alloyed cores at 310 °C for 2 h, we did not observe any noticeable change in PL emission spectra, which supported the alloyed $Cd_{1-x}Zn_xS$ cores with homogeneity rather than $Cd_{1-x}Zn_xS$ cores with chemical composition gradient. Further alloying process caused by intradiffusion of Zn atoms into the inner region

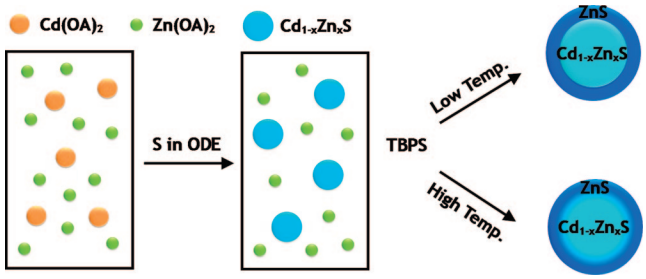

Figure 6. Synthetic scheme and proposed structures of core/shell NCs. $Cd_{1-x}Zn_xS/ZnS$ core/shell NCs grown at higher temperature (above 250 °C) after the second injection of S precursor have diffuse boundary between the core and the shell but $Cd_{1-x}Zn_xS/ZnS$ core/shell NCs grown at lower temperature (at 250 °C) have sharp boundary.

from the composition gradient structure will show blue shift in PL spectra. By simply changing the amount of S precursors in the first injection (S in 1-ODE), we obtain various composition of an alloyed $Cd_{1-x}Zn_xS$ core ($0.49 \leq x \leq 0.76$) with well-defined band edge emission wavelength. After the first injected S precursors are almost consumed, the second S precursors (TBPS) are introduced to passivate the surface of the alloyed cores with ZnS shell layers (wider band gap material). Through the shell formation, the trap emissions of the core are suppressed and thus the strong band edge emission is resulted, indicating the successful passivation of surface-dangling bonds on the $Cd_{1-x}Zn_xS$ alloyed cores with ZnS layer and the effective confinement of excitons within the cores. At the high ZnS shell growth temperature (above 280 °C), Zn atoms located in the ZnS shells can migrate into the $Cd_{1-x}Zn_xS$ core, resulting in high PL QY (up to 80% at room temperature) and better photostability under prolonged UV irradiation.

We tested S in 1-ODE and TBPS precursors in the first and the second steps. When rather lower reactivity of TBPS was introduced in the first injection step, $Cd_{1-x}Zn_xS$ NCs with PL emission wavelengths below 460 nm were hardly obtained. When the higher reactivity of S in 1-OED was used in the second step, its higher reactivity caused unnecessary formation of ZnS nanocrystals rather than epitaxial growth of ZnS shells. Thus we chose S in ODE in the first step injection and TBPS in the second injection step.

In summary, we report a facile synthesis of highly luminescent blue emitting nanocrystals (NCs) in a straightforward and reproducible manner. Prepared NCs exhibit strong band edge PL emissions (photoluminescence quantum yield, PL QY, up to 80%) with narrow spectral bandwidth (fwhm < 25 nm) at room temperature. The NCs possess superb optical properties originating from the successful growth of ZnS overlayers on the $Cd_{1-x}Zn_xS$ cores as well as improved interface between alloyed $Cd_{1-x}Zn_xS$ cores and ZnS shells through the intradiffusion of Zn atoms during the reaction at elevated temperature (310 °C). The emission wavelengths can be precisely tuned by varying the amount of highly reactive S precursors (S in 1-ODE) over the range from violet (415 nm) to blue (461 nm). Moreover, scale-up capability of our synthetic procedure to multigrams (3 g) was also demonstrated.

Acknowledgment. We thank Bonghwan Chon and Taiha Joo at POSTECH for their time-resolved photoluminescence decay profile measurement. This work was financially supported by the Korea Science and Engineering Foundation (KOSEF) through CNNC, the Acceleration Research Program, and the NANO Systems Institute-National Core Research Program (NSI-NCRC). This work was supported in part by MOE through BK21 program and Seoul R&BD program.

CM801201X